Molecular Crystals and Liquid Crystals
Publication details, including instructions for authors and subscription information:
http://www.tandfonline.com/loi/gmcl16

# Behaviour of Nematic Liquid Crystals in Inhomogeneous Electric Fields

V. G. Chigrinov [a] , I. N. Kompanets [a] & A. A. Vasiliev [a]
[a] Lebedev Physical institute, USSR Academy of Sciences, Leninsky prospect 53, Moscow
Version of record first published: 14 Oct 2011.

To cite this article: V. G. Chigrinov , I. N. Kompanets & A. A. Vasiliev (1979): Behaviour of Nematic Liquid Crystals in Inhomogeneous Electric Fields, Molecular Crystals and Liquid Crystals, 55:1, 193-207

To link to this article: http://dx.doi.org/10.1080/00268947908069802

*Mol. Cryst. Liq. Cryst.*, 1979, Vol. 55, pp. 193–208
0026-8941/79/5501–0193$04.50/0

Printed in United States of America



# Behaviour of Nematic Liquid Crystals in Inhomogeneous Electric Fields

V. G. CHIGRINOV, I. N. KOMPANETS, and A. A. VASILIEV
*Lebedev Physical Institute, USSR Academy of Sciences, Leninsky prospect 53, Moscow*

(*Received August 11, 1978; in final form March 23, 1979*)

The behaviour of homogeneously aligned nematic liquid crystal layers in inhomogeneous electric fields has been theoretically and experimentally investigated. The variation of the phase retardation of monochromatic light along nematic liquid crystal layer at the edges of a cell electrode has been obtained. Anisotropic character of the resolution of liquid crystal devices is shown.

## INTRODUCTION

Nematic liquid crystals (NLC) are potentially useful electrooptical materials for displays[1] and space-time light modulators (SLM) for optical information processing.[2,3] One of the most important characteristics of displays and of SLM particularly is spatial resolution. Spatial resolution of certain liquid-crystal devices, e.g. of image converters based on photosemiconductor-liquid crystal structures[4,5] and electrically-controlled diffraction gratings,[6] has been experimentally measured. But, to determine the maximum possible resolution, one should take into account NLC parameters, the aligning technique and the spatial variation of the controlling electric fields, i.e. boundary conditions for the NLC layer. Since the field effects extensively applied in SLM[1,3] have been investigated in detail for the case of homogeneous electric fields, the main difficulty in solving this problem lies, obviously, in the anisotropic interaction of the NLC layer with the substrate surface and inhomogeneous electric field.

In the present paper, a method is proposed for the theoretical and experimental investigation of NLC layer deformation in an inhomogeneous electric field. The possibilities of this method are revealed in studying matrix-addressed phase SLM based on the field effect[7,8] in uniformly aligned NLC layers with positive dielectric anisotropy.

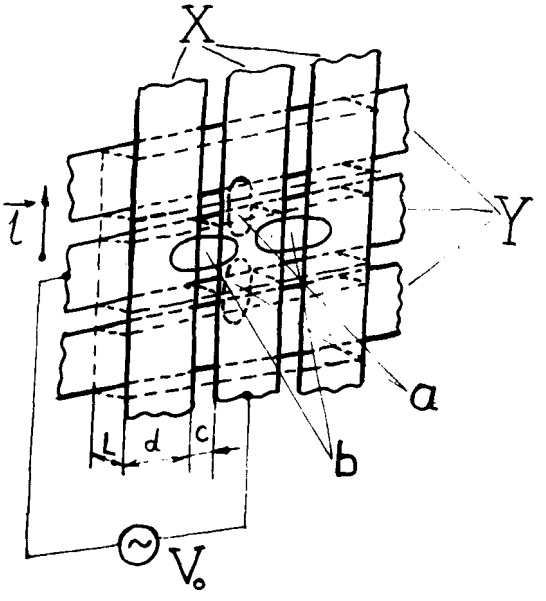


FIGURE 1 Schematic representation of matrix-addressed SLM. l represents the director orientation with no applied voltage.

## BASIC DEFINITIONS

A part of the NLC layer located between cross bar electrodes ("$X$" and "$Y$" electrodes) of the matrix SLM is shown schematically in Figure 1. Suppose the long axes of NLC molecules are homogeneously aligned along $X$-electrodes in the initial state, i.e. with no voltage applied to the electrodes. If the NLC possesses positive dielectric anisotropy, i.e.

$$\Delta\varepsilon = \varepsilon_{\parallel} - \varepsilon_{\perp} > 0 \tag{1}$$

($\varepsilon_{\perp}$ and $\varepsilon_{\parallel}$ are dielectric constants in the perpendicular and parallel directions to the main molecular axis), then the voltage $V$ exceeding the threshold value $V_{\text{th}}$:[9]

$$V_{\text{th}} = \pi\left(\frac{4\pi K_{11}}{\Delta\varepsilon}\right)^{1/2} \tag{2}$$

causes splay deformation[10] in NLC layer. This deformation leads to molecular re-orientation and is characterized by elasticity constant $K_{11}$.

Consider now areas of NLC layer adjacent to edges of the electrodes connected with the power source. Let the width of electrode stripes $d$ and the space $C$ between them meet the requirements:

$$d \gg L; \qquad C \lesssim 3L \tag{3}$$

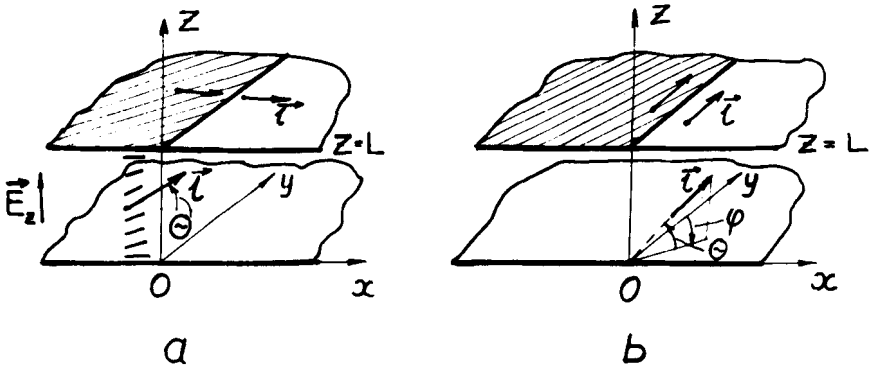


FIGURE 2 Basic geometrical relationships for type "$a$" and type "$b$" regions.

where $L$, is the NLC layer thickness. Then one may neglect the influence of neighbouring electrodes and consider the boundary regions designated in Figure 1 by letters $a$ and $b$ to be semi-infinite capacitors (see Figure 2). Figure 1 shows that two types of orientation of the long molecular axes (director) are realized in matrix SLM, i.e. director is perpendicular to electrode boundaries in $a$-regions, and is parallel to $X$-electrode boundaries in $b$-regions.

As shown in Figure 2 let us choose a rectangular coordinate system $(x, y, z)$ coupled with the boundary of the upper semi-infinite capacitor electrode, so the origin 0 is in the centre of the infinite bottom electrode extending to $\infty$ in both $\pm x$ and $\pm y$ directions. The potential of the infinite electrode is supposed henceforth to be equal to zero and the potential of the semi-infinite electrode is equal to the voltage $V_0$ applied to the cell electrodes. Since the electrode boundary is parallel to the $Y$-axis, the potential distribution $V$ in the NLC layer depends only on $X$ and $Z$:

$$V = V(X, Z) \tag{4}$$

and the electric field component $E_y$ is equal to 0:

$$-\nabla V = \mathbf{E}(X, Z) = \{E_x(X, Z); 0; E_z(X, Z)\} \tag{5}$$

It is convenient to describe space location of director orientation $\mathbf{l}$ by angular coordinates $\theta(X, Z)$ and $\varphi(X, Z)$ (see Figure 2). Obviously, in case "$a$" $\varphi(X, Z) = \pi/2$ at any voltage on the electrodes. In case "$b$" the presence of field component $E_x$ should result in the deviation of $\varphi$ angle from the initial value $\varphi(X, Z) = 0$.

Re-orientation of NLC molecules under the electric field causes appropriate changes of the refractive index of the NLC layer. In this way in SLM the phase or amplitude (with polarizers present) modulation of the passing light is

performed. The phase retardation $\Delta\Phi$ for a collimated monochromatic light beam incident at the normal to NLC layer surface therefore may be calculated by means of the equation equally valid for both *a* and *b* cases:[9]

$$\Delta\Phi(x) = \left(\frac{2\pi}{\lambda}\right) \int_0^L \left[ \frac{n_{\parallel} n_{\perp}}{(n_{\parallel}^2 \sin^2 \theta(x, z) + n_{\perp}^2 \cos^2 \theta(x, z))^{1/2}} - n_{\perp} \right] dz \quad (6)$$

where $n_{\parallel}$ and $n_{\perp}$ are the principal values of NLC refractive index for the light with electric vector parallel or perpendicular to the optical axis respectively. Phase retardation is independent of the angle $\varphi$, which determines only the optical activity of the NLC layer. But the total rotation of polarization plane in our case is equal to zero, since

$$\varphi|_{Z=0} = \varphi|_{Z=L} \quad (7)$$

which follows from (Eq. 14b) (see below).

The resolution of the matrix-addressed SLM is determined by the width of the space-transient region† where the phase retardation changes from $\Delta\Phi_0$, corresponding to homogeneous field (voltage $V_0$ across NLC layer), up to $\Delta\Phi_{max}$, which is equal to :

$$\Delta\Phi_{max} = \frac{2\pi L(n_{\parallel} - n_{\perp})}{\lambda} \quad (8)$$

in regions where electric field is absent.

## CALCULATION OF DIRECTOR SPACE DISTRIBUTIONS AND PHASE RETARDATION IN TRANSIENT REGION

Suppose, the cell is excited by an ac voltage $V \gtrsim V_{th}$ whose frequency $\omega$, is sufficiently high to make it possible to neglect the conductivity currents $\mathbf{j}$ in comparison with displacement currents $\partial\mathbf{D}/\partial t$, i.e.

$$\left|\frac{\partial \mathbf{D}}{\partial t}\right| = \left|\frac{\partial(\hat{\varepsilon}\mathbf{E})}{\partial t}\right| \gg |4\pi\mathbf{j}| = 4\pi|\hat{\sigma}\mathbf{E}| \quad (9)$$

where $\hat{\varepsilon}$ and $\hat{\sigma}$ are dielectric and conductivity tensors respectively. Using a specific type of $\hat{\varepsilon}$ and $\hat{\sigma}$ tensors for homogeneously aligned NLC layer with $\Delta\varepsilon > 0$ one may transform inequality Eq. (9) in the following way:

$$\varepsilon_{\perp}\omega \gg 4\pi\sigma_{\perp} \quad (10)$$

† "Space-transient region" is introduced analogously to transient processes in electric schemes.

In this case the mechanism of NLC molecule re-orientation is purely dielectric, and the free energy of the NLC layer possessing an electric field of the type described in (Eq. 5) is:

$$\mathcal{F} = \frac{1}{2}\int_{-\infty}^{\infty} dx \int_0^L dz \Bigg[ K_{11}\Bigg(\cos\theta\cos\mathcal{S}\frac{\partial\mathcal{S}}{\partial x} - \sin\theta\sin\mathcal{S}\frac{\partial\theta}{\partial x} + \cos\theta\frac{\partial\theta}{\partial z}\Bigg)^2 + K_{22}\Bigg(\frac{\partial\mathcal{S}}{\partial z}\cos^2\theta - \sin\theta\cos\theta\sin\mathcal{S}\frac{\partial\mathcal{S}}{\partial x} - \cos\mathcal{S}\frac{\partial\theta}{\partial x}\Bigg)^2 + K_{33}\Bigg\{\Bigg(\sin\theta\frac{\partial\theta}{\partial z} + \cos\theta\sin\mathcal{S}\frac{\partial\theta}{\partial x}\Bigg)^2 + \cos^2\theta\Bigg(\sin\theta\frac{\partial\mathcal{S}}{\partial z} + \cos\theta\sin\mathcal{S}\frac{\partial\mathcal{S}}{\partial x}\Bigg)^2\Bigg\} - \frac{\varepsilon_\perp}{4\pi E^2} - \frac{\Delta\varepsilon}{4\pi}(E_x E_z \sin 2\theta\sin\mathcal{S} + E_x^2\cos^2\theta\sin^2\mathcal{S} + E_z^2\sin^2\theta)\Bigg] \quad (11)$$

where $k_{ii}(i = 1, 2, 3)$ are elastic constants of NLC.[10]

In steady-state electric fields satisfying Eq. (10), the minimum of the functional Eq. (11) corresponding to the equality between dielectric and elastic moments per unit volume of NLC, can be obtained at $\theta(X, Z)$ and $\mathcal{S}(X, Z)$ which satisfy Euler equation:

$$K_{11}\frac{\partial^2\theta}{\partial z^2} + K_{33}\frac{\partial^2\theta}{\partial x^2} + \frac{\Delta\varepsilon}{4\pi E_x E_z} = 0 \quad (12a)$$

(for the case "$a$" ($\mathcal{S} = \pi/2$)) and

$$k_{11}\frac{\partial^2\theta}{\partial z^2} + k_{22}\frac{\partial^2\theta}{\partial x^2} + (k_{11} - k_{22})\frac{\partial^2\varphi}{\partial x\,\partial z} + \left(\frac{\Delta\varepsilon}{4\pi}\right)(E_z^2\theta + E_x E_z\varphi) = 0$$

$$k_{11}\frac{\partial^2\varphi}{\partial x^2} + k_{22}\frac{\partial^2\varphi}{\partial z^2} + (k_{11} - k_{22})\frac{\partial^2\theta}{\partial x\,\partial z} + \left(\frac{\Delta\varepsilon}{4\pi}\right)(E_x^2\varphi + E_x E_z\theta) = 0 \quad (12b)$$

for the case "$b$".

Equations (12a) and (12b) are linear in $\theta$ and $\varphi$ only for small deviations from the initial position of the director:

$$\sin\theta \sim \theta,\ \cos\theta \sim 1 \quad \text{(case "}a\text{" and "}b\text{")}$$
$$\sin\varphi \sim \varphi,\ \cos\varphi \sim 1 \quad \text{(case "}b\text{")} \quad (13)$$

at any $X$ and $Z$.

The boundary condition corresponding to "strong anchoring" of the director on substrates is:

for the case "$a$"

$$\theta|_{z=0} = \theta|_{z=L} = 0 \tag{14a}$$

for the case "$b$"

$$\begin{cases} \theta|_{z=0} = \theta|_{z=L} = 0 \\ \varphi|_{z=0} = \varphi|_{z=L} = 0 \end{cases} \tag{14b}$$

As $\theta$ and $\varphi$ are the functions of two variables, one must set boundary condition on the closed curve in the plane $(X, Z)$. The fact that at a sufficiently long distance from semi-infinite electrode boundary the electric field in the NLC layer becomes homogeneous can be used to obtain correct boundary conditions, i.e.

$$|\mathbf{E}| = E_z = \frac{4\pi D_z}{\varepsilon_\perp \sin^2\theta + \varepsilon_\parallel \cos^2\theta} \sim \frac{V_0}{L} \quad \text{at } x \to -\infty \tag{15}$$

(this holds if conditions Eq. (13) are observed)

$$|\mathbf{E}| = 0 \quad \text{at } x \to \infty$$

As follows from Eq. (15) for the case "$a$" and "$b$" we have:

$$\theta|_{x\to\infty} = 0; \qquad \theta|_{x\to-\infty} = \theta_0(Z) \tag{16a}$$

Furthermore, for the case "$b$"

$$\mathscr{S}|_{x\to\pm\infty} = 0 \tag{16b}$$

$\theta_0(Z)$ function in Eq. (16a) is the solution of Eq. (12a) with boundary conditions Eq. (14a) in a homogeneous electric field $E \sim V_0/L$ (see, for example.[8,9]

The electric field in the NLC layer satisfies Maxwell equation

$$(\nabla(\hat{\varepsilon}\mathbf{E})) = 0 \tag{17}$$

Under condition Eq. (13), when

$$\Delta\varepsilon \sin^2\theta \ll \varepsilon_\perp \qquad \text{(cases "}a\text{" and "}b\text{")};$$

$$\Delta\varepsilon \sin^2\mathscr{S} \ll \varepsilon_\perp \qquad \text{(case "}b\text{")} \tag{18}$$

Eq. (17) appears in the form

$$\varepsilon_\parallel \frac{\partial^2 V}{\partial x^2} + \varepsilon_\perp \frac{\partial^2 V}{\partial z^2} = 0 \qquad \text{(in the case "}a\text{")};$$

$$\frac{\partial^2 V}{\partial x^2} + \frac{\partial^2 V}{\partial z^2} = 0 \qquad \text{(in the case "}b\text{")} \tag{19}$$

In dimensionless coordinates

$$z' = \frac{\pi z}{L}, \qquad x' = \frac{(\varepsilon_\perp/\varepsilon_\parallel)^{1/2}\pi x}{L} + 1 \qquad \text{(case "}a\text{")}$$

$$Z' = \frac{\pi Z}{L} \qquad X' = \frac{\pi X}{L} \qquad \text{(case "}b\text{")} \tag{20}$$

Eqs. (19) ("$a, b$") are transformed into Laplace equation:

$$\nabla^2 V = \frac{\partial^2 V}{\partial x'^2} + \frac{\partial^2 V}{\partial z'^2} = 0 \tag{21}$$

The solution of Eq. 21 with the boundary condition of the semi-infinite capacitor

$$V|_{z'=0} = 0, \qquad V\Big|_{\substack{z'=L \\ x'\le 0}} = V_0 \tag{22}$$

has the following form;[11]

$$V(X', Z') = \frac{V_0}{\pi a(X', Z')}, \tag{23}$$

where $a(X', Z')$ is derived from the following system of equations:

$$\begin{aligned} X' - 1 &= b + \cos a \cdot \exp(b) \\ Z' &= a + \sin a \cdot \exp(b) \end{aligned}$$

$$0 \le a \le \pi, \qquad -\infty < b < \infty \tag{24}$$

The voltage $V_0$ is chosen for phase retardation $\Delta\Phi_0$ of the passing light with the wavelength of 633 nm to follow the condition:

$$\Delta\Phi_{\max} - \Delta\Phi_0 = \pi \tag{25}$$

corresponding to the maximum depth of phase (or amplitude) modulation.

Finally in the "$a$" case the process of NLC layer deformation in the electric field Eq. (23) is described by the Equation derived from Eq. (12a), taking into account Eq. (20), (2) and the equation of motion for the director (see for example:[8]

$$\frac{\partial\theta}{\partial t'} = \frac{\partial^2\theta}{\partial z'^2} + \beta\frac{\partial^2\theta}{\partial x'^2} + \left(\frac{V_0}{V_{\text{th}}}\right)^2\left[\left(\frac{\varepsilon_\perp}{\varepsilon_\parallel}\right)^{1/2}\frac{\partial a}{\partial x'}\frac{\partial a}{\partial z'} + \theta\left\{\left(\frac{\partial a}{\partial z'}\right)^2 - \frac{\varepsilon_\perp}{\varepsilon_\parallel}\left(\frac{\partial a}{\partial x'}\right)^2\right\}\right] \tag{26}$$

where $t' = k_{11}t/\gamma_1 L^2$, is the normalized dimensionless time ($\gamma_1$ is the coefficient of viscosity, $t$ = time); $\beta = k_{33}\varepsilon_\perp/(k_{11}\varepsilon_\parallel)$.

To solve Eq. (26) numerically one should replace the boundary conditions Eq. (14a) by the approximate boundary conditions, given in a certain finite rectangular region ($x'_L \leq x' \leq x'_U$, $0 \leq z' \leq \pi$):

$$\theta(x'_L, z') = \theta_0(z'), \qquad \theta(x'_U, z') = 0,$$
$$\theta(x', 0) = 0, \qquad \theta(x', \pi) = 0 \tag{27}$$

Small values of the electric field deviation $E_z$ from $(-V_0/L)$ at $x' = x_L$, and from zero at $x' = x_U$, provide the criterion in choosing the boundary conditions.

In order to calculate the director distribution $\theta(X', Z')$, and phase retardation $\Delta\Phi_{max} - \Delta\Phi(X')$, Eq. (26) with boundary conditions Eq. (27) was solved numerically together with Eqs. (6 and 25). The equations were solved with the help of locally-one-dimensional difference scheme.[12]

The calculation of the director distribution for the case "$b$" is a more complicated task. The system of Eqs. (12b) having boundary conditions for $\theta(X', Z')$ which correspond to Eq. (27), and with the boundary conditions on $\varphi(X', Z')$:

$$\varphi(x', 0) = \varphi(x', \pi) = \varphi(x'_L, z') = \varphi(x_U, z') \tag{28}$$

along with Eqs. (6 and 25) was also solved numerically. To solve these equations all the derivatives from Eqs. (12b) were replaced by difference operators, dependent on $\theta$ and $\varphi$ functions in the partition points. The accuracy of the solution of the linear equation system Eq. (9) and the difference scheme convergence was controlled by changing the sampling step along $X'$, and $Z'$.

## EXPERIMENTAL SET-UP

In the experimental matrix space-light modulator[3] a NLC layer with $L = 20$ um was placed between two polished quartz substrates having the dimensions $20 \times 40$ mm$^2$ and with tin dioxide transparent electrode stripes deposited on the substrates (8 "$x$" electrodes and 8 "$y$" electrodes). The electrode stripes were 2 mm wide ($d = 2$ mm), and the distance between them was 100 $\mu$m. We obtained a homogeneous alignment of the NLC layer by rubbing the substrates along "$x$"-electrode.

Obviously, at fixed $\Delta\Phi_0$ the greater the thickness $L$, the more accurately is fulfilled condition Eq. (13). Indeed, the calculations show that the largest value of $\theta$ is obtained at $X < 0$ in the centre of the layer, so

$$\sin \theta_m \propto L^{-1/2} \tag{29}$$

where

$$\theta_m = \max\{\theta(x, z)\} = \theta\Big|_{\substack{x \to -\infty \\ z = L/2}} \tag{30}$$

An increase of the thickness $L$ to the values more than 30 $\mu$m becomes contradictory to the condition Eq. (3) as the distance $C$ is small in the present sample. For a closer correspondence of the experimental conditions to the calculations, cells with special configurations of the transparent electrodes were used. A solid $SnO_2$ electrode was placed on one of the cell substrates. The other electrode occupied only quadrant of substrate surface and had the form of a rectangle ($8 \times 10$ mm$^2$) with the sides parallel and perpendicular to the direction of molecular alignment in the NLC layer. The NLC layer was either 20 or 44 um thick in such cells.

In the experiments, we have used a NLC which is an eutectic mixture of three $n'$-cyanophenyl ethers of $n$-alcylbensoic acids with the melting point $T_{ml}$ of about 18°C, and a clearing temperature $T_{cl} = 70$°C. Mixture parameters[13] are listed in Table I. The same parameters have been used for calculations.

The scheme of the experimental installation is presented in Figure 3. A He–Ne laser beam 1 passed through polarizer 2, liquid crystal cell 3 (used as a controlled compensator) and was normally incident upon the experimental sample. A 100 times magnified image of the NLC layer was formed by the microscope objective 7.

The voltage on the cell-compensator electrodes is chosen for $\Delta\Phi_c$ phase retardation of the light passing through the compensator to meet the condition:

$$\Delta\Phi_c \neq \Delta\Phi_{max} = 2\pi n, \qquad n = 0, 1, 2, \ldots \tag{31}$$

where $\Delta\Phi_{max}$, is determined by expression 8.

TABLE I

NLC mixture parameters at 25°C

| | | |
|---|---|---|
| Dielectric constants | $\varepsilon_{\parallel}$ | 31 |
| | $\varepsilon_{\perp}$ | 9.26 |
| Dielectric anisotropy | $\Delta\varepsilon$ | 21.74 |
| Elasticity constants (poise) | $K_{11}$ | $0.675.10^{-6}$ |
| | $K_{22}$ | $1.050.10^{-6}$ |
| | $K_{33}$ | $1.510.10^{-6}$ |
| Viscosity coefficient (dyne) | $\gamma_1$ | 2.5 |
| Threshold voltage-effect (B) | $V_{th}$ | 0.59 |
| Refractive indexes: | | |
| Common | $n_{\perp}$ | 1.509 |
| ncommon | $n_{\parallel}$ | 1.654 |

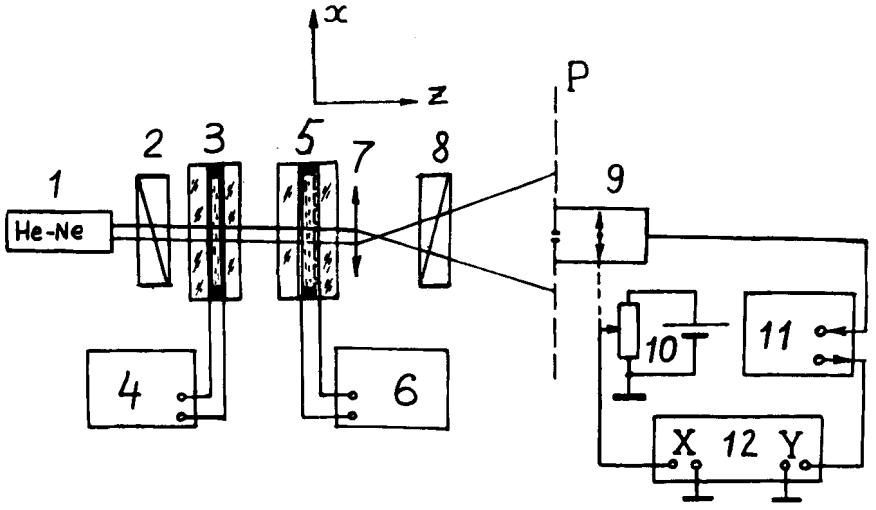


FIGURE 3 Scheme of an experimental installation. 1-laser; 2-polaryzer; 3-LC cell (compensator); 4,6-controlled AC voltage generator; 5-experimental sample; 7-microobjective × 10; 8-analyser; 9-photomultiplier; 10-variable resistor of the shift detector; 11-dc amplifier; 12-two-coordinate recording potentiometer.

When polaryzer 2 and analyser 8 are crossed, condition Eq. (31) corresponds to the intensity minimum of the experimental sample image with no voltage applied to its electrodes. For an electrode voltage $V_0$ the intensity $I$ in the $P$ plane is:

$$I = I_0 \sin^2\left(\Delta\Phi \frac{x/m}{2}\right); \tag{32}$$

where $x$ is the coordinate in the NLC layer plane, the scale factor $m$ is equal to the magnification of the optical system; and $I_0$, is the maximum measured intensity.

The light intensity spatial distribution in the magnified image of the transient region was measured by means of moving along the $x$-axis photomultiplier 9 whose entrance pupil diameter was about 50 um. The variable resistor 10 was used as the position detector, and its signal was applied to the "$X$" input of the two-coordinate recording potentiometer 12. The photomultiplier signal was applied to the "$Y$" input of the potentiometer through the dc amplifier 11.

## RESULTS

The theoretical and experimental curves for phase retardation distribution in the transient region of the sample under investigation are plotted in Figure 4 for "$a$" and "$b$" cases. Good agreement is achieved in case "$a$" between the

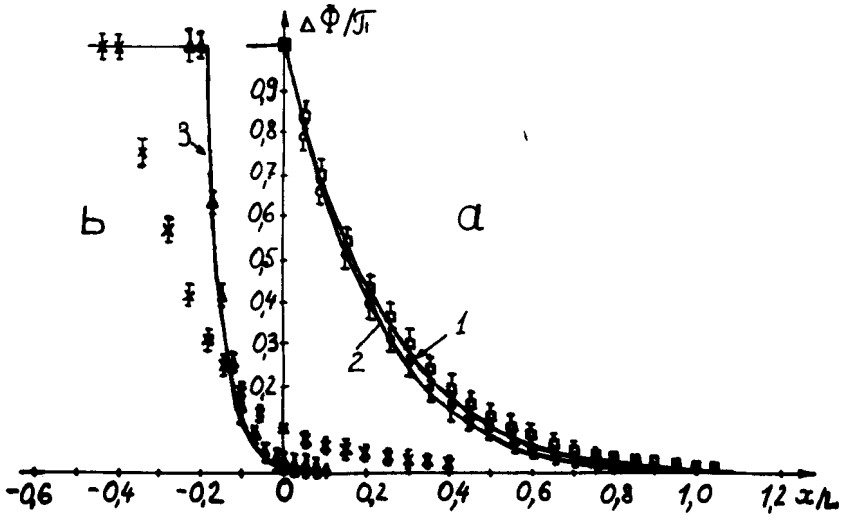


FIGURE 4 Phase retardation distribution in the transient region: $a$-the electrode boundary is perpendicular; $b$-the electrode boundary is parallel to the initial director orientation; calculated curves (dense) 1 and 3-$L$ = 20 $\mu$m; 2 and 3-$L$ = 44 $um$. Experimental data: ○ and △ $L$ = 44 um, □ and × $L$ = 20 um.

calculated curves (dense curves) and the experimental results which are obtained by means of recalculating the intensity distributions in formula Eq. (32). Averaging was performed for data obtained in different parts of the transient regions in two experimental samples. Averaged distributions were approximated by exponents with the help of least squares fitting. Approximation was performed numerically by a computer (see, for example).[14] Discrepancy in the calculated and experimental data does not exceed the experimental error of 12%. As seen from diagrams, the width of the transient region, which was measured as the length of the curve drop $\Delta\Phi(x)/\pi$ from 0.99 to 0.01 (for the case "$a$") was approximately equal to the layer thickness $L$. However, the intensity transient region is somewhat narrower and constitutes according to the same criterion $0.6L$. The shape of the phase retardation curve drop is very close to the exponential one. Maximum slope of the curve is observed in the vicinity of $X' = 0$.

In the case "$b$" the calculated values $\Delta\Phi(x)$, described in coordinates $X/L$, practically coincide for the both values of $L$. Also the theoretical width of the transient region does not exceed $0.2L$. This may be probably explained by a small value of the "source function" in the system of Eq. (12b), namely

$$\left(\frac{\Delta\varepsilon}{4\pi}\right)(E_x^2\theta + E_xE_z\varphi), \qquad \left(\frac{\Delta\varepsilon}{4\pi}\right)(E_x\varphi + E_xE_z\theta)$$

Due to assumed small values of the angles $\theta$ and $\varphi$ these terms are small everywhere, except some area in the vicinity of the point with coordinates $x = 0$, $Z = L$. However, since the layer thickness is 20 um, $\theta_m \sim 26°$, and condition Eq. (13) is violated. Satisfactory coincidence with the experiment is observed only at the thickness $L = 44$ um, when $\theta_m \sim 17°$.

The source function for the Eq. (12a) in the case "$a$" is equal to

$$\left(\frac{\Delta\varepsilon}{4\pi}\right)E_x E_z$$

which in linear approximation does not depend on angle $\theta$. Therefore, good agreement of experimental data with the calculated ones is observed for both thicknesses of NLC layer.

The source functions in Eq. 12 are directly proportional to dielectric anisotropy. This implies that the width of the transient region must increase with the increase of $\Delta\varepsilon$. The dependence of the resolution on the value of dielectric anisotropy has been proved by experiments with the liquid crystal-photoconductor structure.[17]

The solution of Eq. (12a) is nontrivial even at zero boundary conditions, when $\theta_0(Z') = 0$ (see Eq. (16a)), Here we come to an important conclusion that in the case "$a$" there is no threshold for NLC deformation in the electric field. This may be caused by the presence of a non-zero electric field component $E_x$ along the initial orientation of the director. Together with the results of other published theoretical[15] and experimental[16] papers, this fact

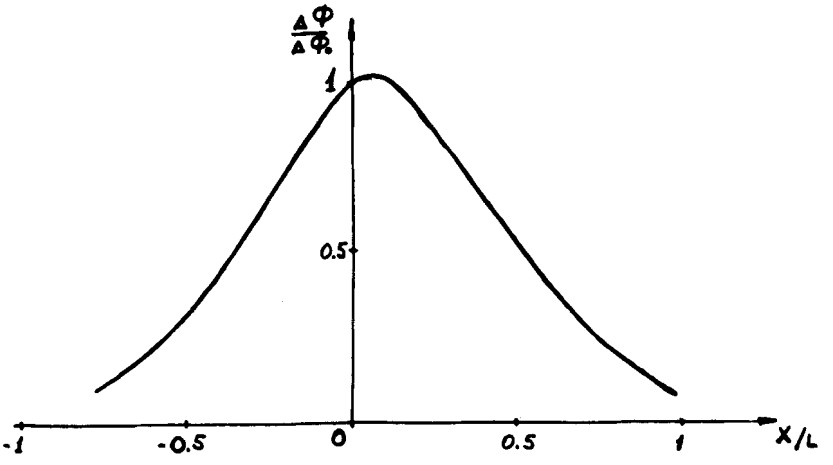


FIGURE 5 The dependence of the phase retardation as a function of the coordinate $X$ for the case " " at voltage 0.295 V on one of the cell electrodes. This is the no threshold case.

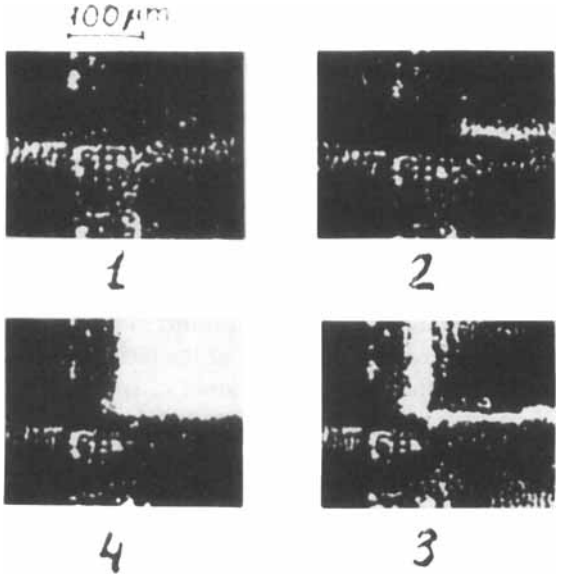


FIGURE 6 Transient image in crossed polarizers at different voltage on matrix SLM electrodes. The case "$a$" is realized at horizontal boundary; and "$b$" case is realized at vertical boundary; $1 - V_0 = 0; \Delta\Phi_0 = 0; 2 - V_0 = 0.295\ V$ (no threshold in "$a$" case; $3 - V_0 = 0.714\ V; \Delta\Phi_0 = \pi$; $4 - V_0 = 0.965\ V; \Delta\Phi_0 = 2\pi$.

allows us to make general conclusion, that irrespective of the deformation character (splay, bend, twist) the threshold voltage exists only when the electric field does not have a component parallel to the direction of the largest dielectric constant for the NLC in an unperturbed state. In the case "$b$" the electric field is perpendicular to the initial orientation of the director and the threshold voltage exists.

In Figure 5 we have presented the dependence of the phase retardation as a function of the coordinate $X$ (for the case "$a$"), which was calculated at voltage $V_{th/2} = 0.295$ V on a semi-infinite cell electrode with the NLC layer thickness being 20 um. The curve has its maximum in the vicinity of the electrode boundary $X' = 0$, where the calculated values of the electric field component

$$E_x = -\frac{\partial V}{\partial x}; \qquad E_z = -\frac{\partial V}{\partial z}$$

become infinite. The absence of the threshold in the case "$a$" is also confirmed by a photo presented in Figure 6.[1]

## CONCLUSION

In the present paper the deformation of a homogeneously aligned NLC layer in an inhomogeneous electric field of a semi-infinite capacitor is theoretically and experimentally studied. The calculation and experimental results show that the maximum available resolution of matrix-addressed phase space-time-light modulator, which is based on NLC field effects, is determined by the dielectric and elastic properties of the liquid crystal, and by the boundary conditions on the layer surface. The width of the transient region at the boundary of the switched on SLM element does not exceed the width of the NLC layer. The different initial director orientations relative to the electrode boundary, and the anisotropic interaction of the electric field and the NLC layer are responsible for the anisotropic nature of spatial resolution.

Despite the limited application of the theoretical model (deformation linearity, certain arbitrariness in choosing boundary conditions for solving the initial equations, no evaluation of the influence of neighbouring SLM electrodes on resolution) the shape and width of the transient region obtained by calculations are in good accord with the experimental data.

Common properties intrinsic to all field effects in NLC enable one to hope that the theoretical model and experimental technique considered will be useful for determining resolution capacity of liquid crystal devices using different field effects and addressing techniques.

## References

1. L. A. Goodman, *RCA Review*, **35**, 613 (1974). *Nonemissive Electrooptic Displays*, edited by A. R. Kmetz and F. K. Won Willisen (Plenum Press, New York and London).
2. D. Casasent, *Proc. IEEE*, **65**, 143 (1977).
3. I. N. Kompanets, A. A. Vasiliev, and A. G. Sobolev. In: *Optical Information Processing* (USA-USSR Seminar, Washington, 1975) (Plenum Publishing Co., 1976), p. 129.
4. J. D. Margerum, *et al.*, *Appl. Phys. Lett.*, **19**, 216 (1971).
5. A. Jacobson, *et al.*, *Opt. Eng.*, **43**. 217 (1975).
6. V. A. Tsvetkov, N. A. Morozov, and M. I. Elinson. *Preprint of Radioelectronic Institute*, **N21**, (170), Moscow, 1974.
7. H. Gruler, T. J. Sheffer, and G. Meier, *Z. Naturforsch.*, **27a**, 966 (1972).
8. P. D. Berezin, *et al.*, *Sov. Phys.—JETP*, **37**, 305 (1973).
9. H. J. Deuling, *Mol. Cryst. Liq. Cryst.*, **19**, 123 (1972).
10. F. C. Frank, *Disc. Faraday Soc.*, **25**, 19 (1958).
11. A. N. Tikhonov and A. A. Samarsky. *Uravneniya matematicheskoy fiziki*, Moscow, Nauka, 1972.
12. A. A. Samarsky, *Vvedenie v teoriyu raznostnykh skhem*, Moscow, 1971; S. N. Godunov and V. S. Ryaben'kii. *Raznostnye skhemy*, Moscow, 1973.
13. M. F. Grebenkin, V. A. Siloverstov, L. M. Blinov, and V. G. Chigrinov, *Kristallografiya*, **20**, 984 (1975).
15. V. G. Chigrinov and M. F. Grebenkin. *Kristallografiya*, **20**, 1240 (1975).

16. A. Rapini and M. Papoular, *J. Phys.*, **30**, 54 (1969); H. Gruler and G. Meier, *Mol. Cryst. Liq. Cryst.*, **16**, 299, (1972).
14. S. Brandt, *Statistical and Computational Methods in Data Analysis* (Heidelberg University, Amsterdam, 1970).
17. A. A. Vasiliev, *Thesis for Candidates Degree* (in Russian), Lebedev Physical Institute, Moscow, 1978.